Strain-Sensing Elastomer/Carbon Nanofiber "Metacomposites"

ARTICLE *in* THE JOURNAL OF PHYSICAL CHEMISTRY C · JULY 2011

Impact Factor: 4.77 · DOI: 10.1021/jp202999c

4 AUTHORS:

Jiahua Zhu
University of Akron
132 PUBLICATIONS **2,565** CITATIONS
SEE PROFILE

Suying Wei
Lamar University
228 PUBLICATIONS **4,496** CITATIONS
SEE PROFILE

Jongeun Ryu
University of California, Los Angeles
24 PUBLICATIONS **944** CITATIONS
SEE PROFILE

Zhanhu Guo
University of Tennessee
367 PUBLICATIONS **6,413** CITATIONS
SEE PROFILE

THE JOURNAL OF PHYSICAL CHEMISTRY C

ARTICLE

pubs.acs.org/JPCC

Strain-Sensing Elastomer/Carbon Nanofiber "Metacomposites"

Jiahua Zhu,[†] Suying Wei,[‡] Jongeun Ryu,[§] and Zhanhu Guo*[,†]

[†]Integrated Composites Laboratory (ICL), Dan F. Smith Department of Chemical Engineering, Lamar University, Beaumont, Texas 77710, United States

[‡]Department of Chemistry and Biochemistry, Lamar University, Beaumont, Texas 77710, United States

[§]Department of Mechanical and Aerospace Engineering, University of California Los Angeles, Los Angeles, California 90095, United States

ABSTRACT:

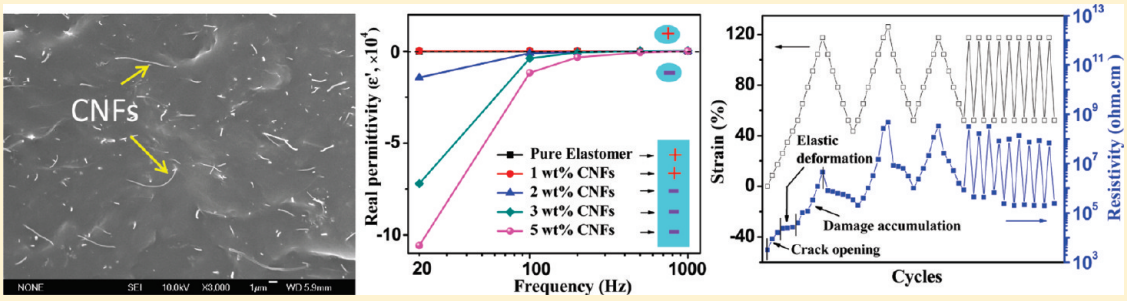

Electrically conductive elastomer nanocomposites reinforced with 1, 2, 3, and 5 wt % carbon nanofibers (CNFs) have been fabricated from two slightly different elastomers (VM1, VM2). The electrical and dielectric percolation threshold of 1 wt % in VM2 nanocomposites is much lower than 3 wt % in the VM1 nanocomposites. Unique negative permittivity is observed in the composites with the CNF concentration correlating well with the percolation thresholds. About 40% unrecoverable strain loss and a permanently increased resistivity by about 2 orders of magnitude are observed due to the formation and opening/closing of the cracks during the first cyclic loading. In the subsequent stretching cycles, the reversible resistivity at 120% strain is about 2−3 orders of magnitude higher than that at 40% strain. Higher fraction of ethylene is found to reduce the thermal stability of the propylene portion in the elastomer. An enhanced thermal stability of the elastomers is observed in both nanocomposite systems; however, the CNFs affect the glass transition and melting behaviors in an opposite way in the two different nanocomposite systems arising from the dispersion quality difference. Melting enthalpy from differential scanning calorimetry (DSC) reveals that the CNFs play a more important role in the VM2 crystallization than that in VM1 composites.

1. INTRODUCTION

The rapid development of multifunctional polymer nanocomposites (PNCs) has opened a new perspective for designing smart materials.[1−6] The unparallel advantages such as cost-effective processability, light weight, and designable multifunctionalities of the PNCs as compared to the conventional smart materials show great potentials in various applications. For example, PNCs are able to improve the response speed and reduce the density of the shape memory alloys,[7,8] introduce flexibility and toughness of the electroactive ceramics,[9,10] and enlarge the actuation forces and mechanical energy density of the electroactive polymers.[11]

The remarkable developments of the carbon nanotubes (CNTs) related research projects have aroused great interest among researchers because of their excellent mechanical, electrochemical, and other physical properties. These outstanding advantages push CNTs to some applications, such as high-strength composites, energy storage, and energy conversion devices and hydrogen storage media.[12] Since the discovery of the piezoresistive response theoretically and experimentally in 1990s, the CNTs have triggered significant expansion in the sensing applications. For example, single-walled CNTs (SWCNT) have the potential to be a strain/stress sensor by either relating the strain/stress of the nanotubes to the sharp change of the conductance[13] or relating to the Raman band shift.[14] It has been possible to develop nanoelectromechanical sensors because the strong dependence of the SWCNT's band structure on the mechanical deformation, such as the well-developed pressure sensors.[15] In addition, CNT-based PNCs were also developed as structural damage sensors in composites.[16,17] Carbon nanofibers (CNFs), with their relatively lower manufacturing cost and excellent electrical conductivity (σ), are promising as effective fillers for PNCs compared to CNTs.[18] Most of the current research on the CNF-based PNCs has been focused on the percolation thresholds at a few weight and volume percentages with an aim to obtain the σ and to explain the conduction mechanisms.[19,20] In spite of the recent progress on the piezoresistive behavior of the CNFs/polypropylene (PP),[21] the

Received: March 31, 2011
Revised: May 1, 2011
Published: June 17, 2011

elastomer-based PNC strain sensors have rarely been reported,[1,22] especially with large-scale mechanical deformation and appreciable sensitivity.

Thermoplastic elastomers have gained considerable significance recently, because they offer combined characteristics of rubber and plastic, which are critically important for the application of a good engineering thermoplastic material. However, the mechanical behavior of the elastomeric materials is very complicated due to their nonlinear response induced by many factors such as stress-softening effect, high deformability, and quasi-incompressibility.[23,24] Regardless of the complexity of the elastomers, such as an unrecoverable hysteresis energy loss induced by the molecular nature of the elastomers, the electrically conductive elastomer composites are valued as the prospective large-size flexible stretch sensors for detecting dangerous deformations and vibrations of vehicle parts.[25] In this case, distinguishable and reversible resistance change depending on stretching should be obtained in these conductive PNCs.

Metamaterials are of great interest due to their unique negative physical properties such as refractive index and permittivity, which can be applied in cloaking, superlens, wave filters, remote aerospace applications, and superconductors.[26−28] It is well recognized that the unusual dielectric property arises from the special periodic structures rather than the composition of the materials. For the polymer-based metamaterial systems, polymers usually served as the insulating hosts or substrates.[29] On the contrary, a unique composition- and processing-dependent negative permittivity at low frequency is discovered in the conductive polymer based PNCs,[30,31] which are termed as "metacomposites". Similar negative permittivity was also observed in the polyimide/CNFs PNCs.[32] However, there are scarce reports on the negative permittivity in the elastomer systems, especially with the capability to sense the strain variation.

In this work, two elastomers with slightly different compositions have been used as the hosting polymer matrix to fabricate conductive PNCs reinforced with CNFs via the solvent-assisted casting method. The dielectric performance of the PNCs based on these two elastomers has been compared. Unique negative permittivities are observed in both composite systems. Appreciable resistivity switching upon applying an extremely large strain is observed, which is essentially important for sensing applications.

2. EXPERIMENTAL SECTION

2.1. Materials. Propylene-based elastomers, Vistamaxx 6102FL (VM1, ethylene content 16 wt %, propylene 84%; melting index 1.3 g/10 min; density 0.862 g/cm^3) and Vistamaxx 6202FL (VM2, ethylene content 15 wt %, propylene 85%; melting index 7.4 g/10 min; density 0.861 g/cm^3), were supplied by Exxon-Mobil Chemical Co. Melting index is a way to compare the melt flow in a thermoplastic melt and is roughly inversely proportional to the viscosity of the melt. The larger melting index in VM1 indicates a lower viscosity than that of VM2. Vapor-grown carbon nanofibers (CNFs, grade PR-24-XT-LHT, Pyrograf Products, Inc.) were heat treated at about 1500 °C to convert the deposited carbon present on the fiber surface to a short-range ordered structure, aiming to provide higher σ. The CNFs are reported to have an average diameter of 100 nm and length of 50−200 μm. The density of the CNFs is reported to be 1.95 g/cm^3.[33] The solvent xylene (laboratory grade) was purchased from Fisher Scientific. All the chemicals were used as-received without any further treatment.

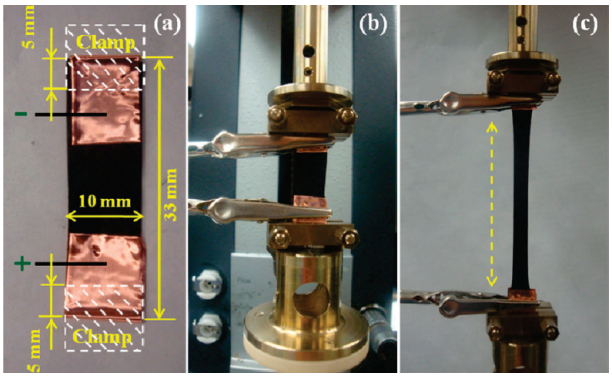

Figure 1. (a) Sample dimensions, (b) clamping system in the DMA setup with 0% elongation, and (c) stretching with 186% elongation.

2.2. Nanocomposites Fabrication. Elastomer (VM) is initially added in xylene with a weight ratio of 1:10 (4 g, 41 mL) and magnetically stirred for 24 h at ∼138 °C until VM is completely dissolved. Then CNFs are weighed as 0.040, 0.082, 0.124, and 0.211 g, which correspond to the weight (volume) ratio of 1 (0.44), 2 (0.89), 3 (1.35), and 5 (2.27) wt (vol) % with regard to pure VM, respectively. The prepared VM xylene solution is then transferred to the CNFs-containing beakers. The mixture is kept overnight without stirring to completely wet the nanofiber surface. Mechanical stirring (500 rpm) is then performed at room temperature for 10 min and followed by magnetic stirring at 138 °C overnight. The resulting PNC solutions are then subjected to ultrasonication for 0.5 h and transferred to a flat mold to allow the solvent evaporation for 24 h. Finally, the PNC thin films with a thickness about 500−600 μm are prepared and ready for the strain-resistivity testing after cutting into rectangular-shaped samples (33 × 10 × 0.5 mm).

2.3. Characterizations. The strain/resistivity measurements are performed on a dynamic mechanical analysis (DMA) fixture using an AR 2000ex (TA Instrumental Co.). As shown in Figure 1, the samples are covered with a piece of conductive copper tape (CU-35C, 3M) at both ends (Figure 1a) to provide an efficient contact with the electrodes and then fixed on the DMA fixture. Two electrodes (alligators) are connected to measure the resistivity (Figure 1b). The strain is precisely controlled by adjusting the gauge length between the two holding clamps, and the resistivity is measured for each strain variation using Agilent 4339B high-resistance meter along the length direction. This equipment allows resistivity measurement from 10^3 up to 10^{16} ohm. The source voltage is maintained at 0.1 V to avoid the current overload. The resistivity is recorded on both stretching and recovery processes.

The dielectric properties of the CNFs/VM PNC thin films are measured by a LCR meter (Agilent, E4980A) equipped with a dielectric test fixture (Agilent, 16451B) in the frequency range of 20−2 M Hz.

The thermal stability of the CNFs/VM PNCs is studied by thermogravimetric analysis (TGA, TA Instruments TGA Q-500) from 25 to 800 °C with an air flow rate of 60 mL/min and a heating rate of 10 °C/min. Differential scanning calorimeter (DSC, TA Instruments Q2000) measurements are carried out under a nitrogen flow rate of approximately 100 mL/min at a heating rate of 10 °C/min from 0 to 200 °C.

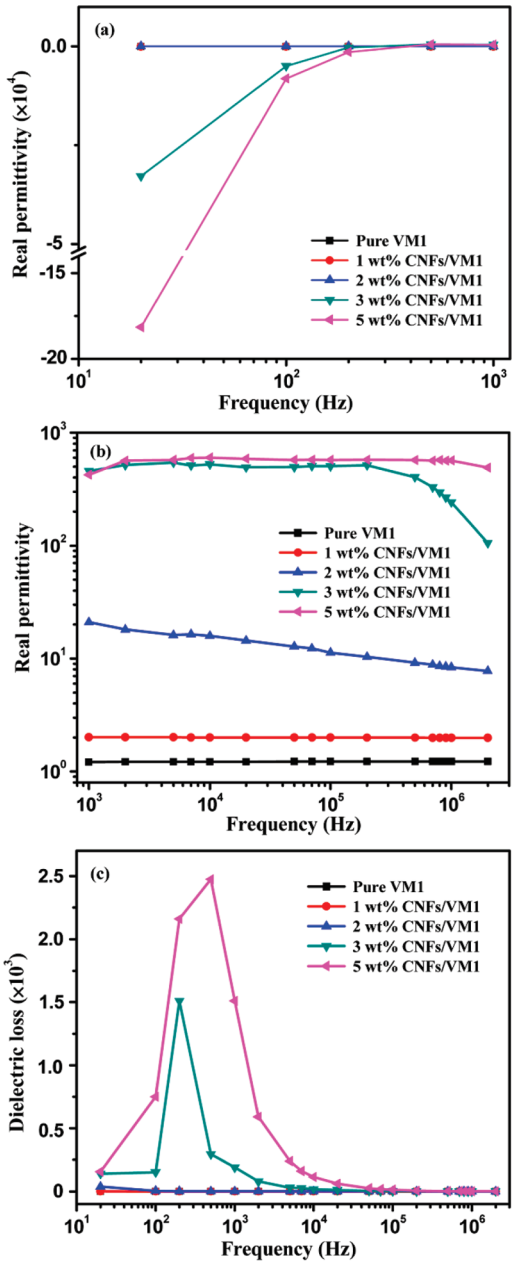

Figure 2. Real permittivity of the CNFs/VM1 PNCs in the frequency range of (a) 20−10^3 Hz and (b) 10^3 to 2 × 10^6 Hz, and (c) dielectric loss of PNCs as a function of frequency. The data points for VM1, 1, and 2 wt % CNFs/VM1 are overlapped in (a) and (c).

3. RESULTS AND DISCUSSION

3.1. Dielectric Property. Figure 2 shows the dielectric property as a function of frequency for pure VM1 and its PNCs with different nanofiber loadings at room temperature. Figure 2, a and b, shows the real permittivity (ε') of the PNCs within the frequency range of 20−10^3 Hz and 10^3 to 2 × 10^6 Hz, respectively.

The ε' of pure VM1 and its PNCs filled with 1 and 2 wt % CNFs shows a positive value at lower frequencies (<10^3 Hz). However, it is interesting to observe negative permittivity (Figure 2a) in the PNCs with nanofiber loading increasing to 3 and 5 wt %. The higher nanofiber loadings induce larger negative values of ε'. For example, the PNCs filled with 3 and 5 wt % CNFs exhibit a value of −3 × 10^4 and −1.8 × 10^5 at the frequency of 20 Hz, respectively, which is attributed to the large resonance induced by the electric field.[34] This negative permittivity disappears when the applied frequency approaches 1000 Hz; similar results were also observed in polypyrrole/WO_3[31] and polyaniline/WO_3[30] PNCs fabricated using a surface-initialized polymerization (SIP) method. In a recent study, negative permittivity was also observed in the polyaniline/epoxy PNCs fabricated from an absorption-transferring process.[35] The occurrence of negative permittivity results from the formation of a continuous conductive network of polyaniline. In this work, the appearance of negative ε' at lower frequency (Figure 2a) observed in the PNCs filled with 3 and 5 wt % CNFs indicates a distinct structural transition of the PNCs when the loading increases to 3 wt %, i.e., percolation phenomena. This behavior is due to the percolated CNFs, i.e., a constructed long-range connectivity among the CNFs. Moreover, it is well-known that the interfacial polarization is determinant to the motion of electrons at the interface. The higher nanofiber loading introduces lots of active interfaces between conductive CNFs and nonconductive polymer matrix within the composites. Under an electric field, a large number of charge carriers are accumulated at the internal interfaces and result in the sharp increase in permittivity, which is often called "Maxwell−Wagner−Sillars effect".[36]

In Figure 2b, the ε' for pure VM1 and its PNCs with 1 wt % nanofiber loading is stabilized at 1.2 and 2.0, respectively, within the frequency range from 10^3 to10^6 Hz. Increasing the nanofiber loading to 2 wt % enhances the ε' to higher value, which starts at 20 (10^3 Hz) and gradually decreases to 8 (10^6 Hz). The steplike decrease of the ε' toward high frequency is induced by the dielectric relaxation, which suggests that the established percolation network structure is not stable and easily affected by the external frequency disturbance, similar to the multiwalled carbon nanotubes/poly(vinylidene fluoride) nanocomposites.[37] Much higher ε' of about 500 is observed in the PNCs with CNF loading higher than the percolation threshold value. The dielectric relaxation appears at higher frequencies with the increase of the nanofiber loading and it almost disappears at the loading of 5 wt %.

Figure 2c shows the dependence of the dielectric loss (tan δ) on the frequency. The tan δ is stabilized at lower than 2 for pure VM1 and its PNCs with 1 and 2 wt % CNFs. A sharp resonance peak (or tan δ peak) is observed in the dielectric loss curve for the PNCs filled with 3 and 5 wt % CNFs, which is well corresponding to the permittivity switching from negative to positive. During this switching process, the charges in the composites much be displaced and the subsequent energies required to complete this process in the form of dielectric loss will be larger than the required energy for the other frequency range.

Figure 3 shows the real permittivity and dielectric loss of pure VM2 and its PNCs with various CNF loadings. Compared to the results from VM1 and CNFs/VM1 PNCs, the negative ε' (<10^3 Hz) appears at a lower filler loading of 1 wt % (Figure 3a) and a correspondingly sharp jump of positive ε' is observed at the same loading (Figure 3b). Together with the results from the resistivity in the following section, it is reasonable to conclude that the percolation threshold of CNFs/VM2 system appears at a lower CNFs loading as compared to that in CNFs/VM1 system, which is due to a better dispersion of the CNFs in the polymer matrix (Figure 5). The ε' increases gradually with increasing CNF loading in both composite systems, and the ε' values after percolation (3 and 5 wt %) are quite similar to each other, which stabilizes at about 400 and 500, respectively. Figure 3c shows the dependence

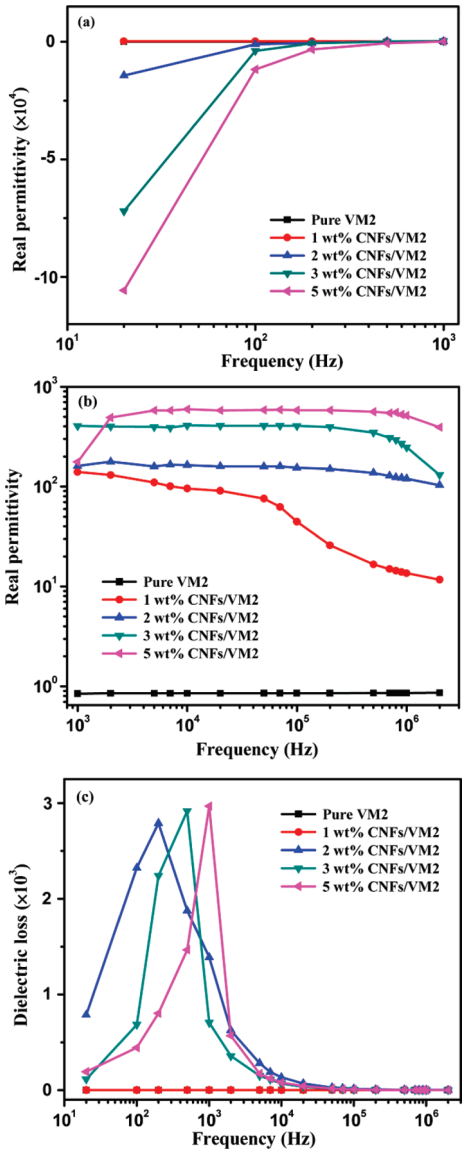

Figure 3. Real permittivity of the CNFs/VM2 PNCs in the frequency range of (a) $20-10^3$ Hz, (b) 10^3-10^6 Hz, and (c) dielectric loss of PNCs as a function of frequency. The data points for VM2 and 1 wt % CNFs/VM2 are overlapped in (a) and (c).

of the dielectric loss ($\tan\delta$) on the frequency for the CNFs/VM2 PNCs. The resonance peaks are observed in the CNFs/VM2 PNCs at the CNF loadings starting from 2 wt %, which is lower than that in the CNFs/VM1 PNCs (3 wt %). In addition, the peak magnitude is relatively larger than that observed in CNFs/VM1 PNCs indicating a larger plasmon resonance in the CNFs/VM2 PNCs.

3.2. Resistivity Measurement. Figure 4 shows a comparison of the CNF loading dependent resistivity in the PNCs with different polymer matrix of VM1 and VM2, respectively. The resistivity of the PNCs is strongly related to the dispersion of the conductive fillers in the polymer matrix.[38,39] In CNFs/VM2 PNCs, Figure 5, b and d, the CNFs are mainly separated individual nanofibers arising from the good dispersion, which leads to a lower percolation threshold at ~1 wt %. The resistivity of the CNFs/VM1 PNCs keeps unchanged until the loading reaches 3 wt % where a reduction of resistivity by about 9 orders of magnitude

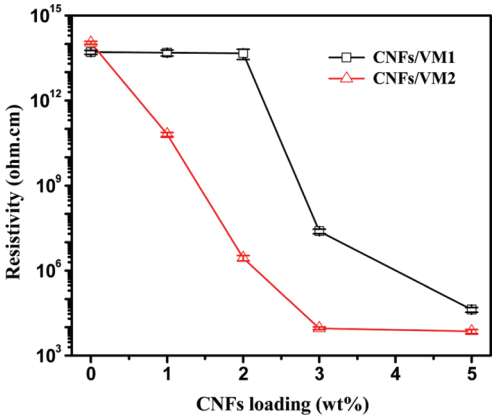

Figure 4. Resistivity of the PNCs with different CNF loadings.

(from 5×10^{13} to 4.2×10^{4} ohm·cm) is observed. This behavior is indicative of percolation phenomena in the CNFs/VM PNCs.

The percolation threshold for the CNFs/VM1 PNCs is observed to be 2−3 wt %, while it is below 1 wt % for the CNFs/VM2 PNCs since a significant reduction of the resistivity is observed with these CNF loadings. The resistivity of the CNFs/VM2 PNCs decreases linearly from 10^{14} to 10^{4} ohm·cm with the increase of the CNF loading from 1 to 3 wt % and is stabilized at 10^{4} ohm·cm while the CNF loading is further increased to 5 wt %. The sharp decrease of the resistivity is due to the formation of the interconnected network among the CNFs. Once the network is formed, a pathway is created to facilitate the electron transportation among CNFs. Balberg et al.[40] defined a relationship between the aspect ratio L/r, where L and r are the length and radius of an individual nanofiber, and the percolation threshold (P_c) in the isotropic case of the randomly distributed sticks: $(L/r)P_c \approx 3$. According to the measured percolation threshold below 1(0.44) wt (vol) % for the CNFs/VM2 PNCs, the expected aspect ratio should be larger than 682, which is lying between the value of individual CNFs ($L/r \approx 500-2000$). Thus, the electron conduction in the CNFs/VM2 PNCs is essentially carried out through the individual CNFs. However, the percolation is 2−3 wt % (0.89−1.35 vol %) for the CNFs/VM1 PNCs, the expected aspect ratio should be lying between 222 and 337, while it is unfortunately out of the range of predicated aspect ratio of 500−2000 for the individual CNFs. This result is in agreement with the SEM image: the CNFs are less uniformly dispersed and some bare polymer areas existed in the CNFs/VM1 PNCs as compared to the CNFs/VM2 PNCs, even though a much lower P_c is reported below 0.1 wt % for the CNTs reinforced PNCs, due to the extremely high aspect ratio between 5000 and 50 000 of CNTs.[41,42] This work provides a solid evidence to support the polymer matrix dependent electrical percolations as well as the consistency between experimental observations and theoretical predictions.

Moreover, it is interesting to observe that the sharp decrease in the resistivity corresponds well to the sharp jump in the permittivity, as observed in Figures 2b, 3b, and 4. The large increase of ε' from 20 to 400 at the frequency of 1000 Hz corresponds to the dramatic decrease of the resistivity from 5×10^{13} to 4.2×10^{4} ohm·cm for the CNFs/VM1PNCs when the CNF loading increases from 2 to 3 wt %. For CNFs/VM2 PNCs at the same frequency, the ε' jump starts from 1 wt % CNF loading with an enhancement by 2 orders of magnitude. Meanwhile, the resistivity is decreased by 3 orders

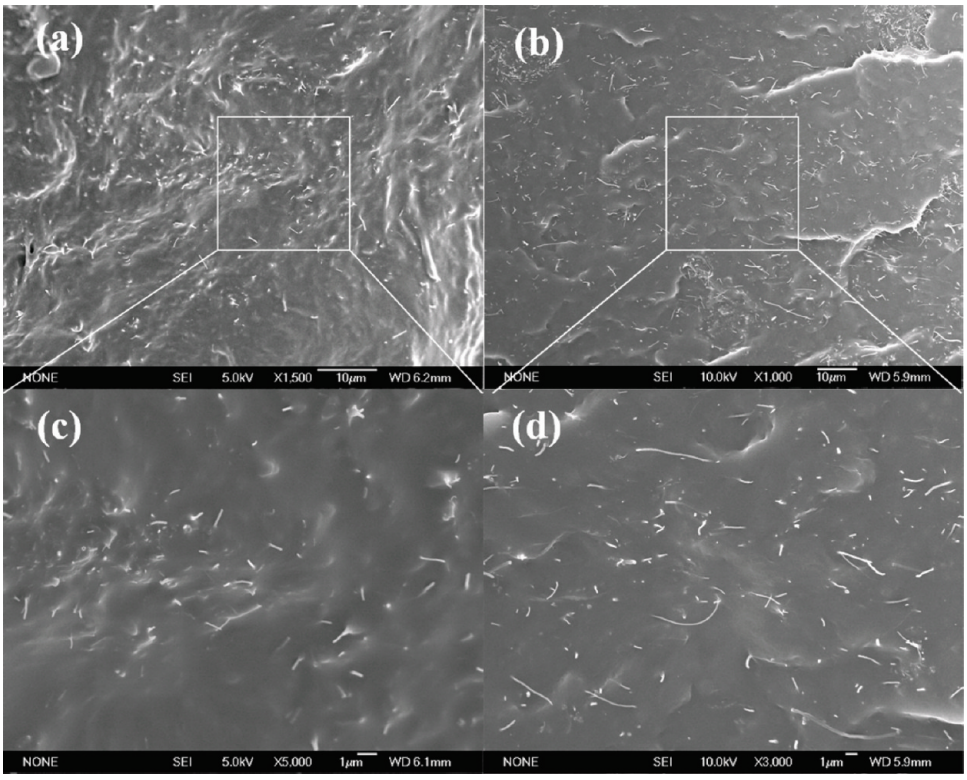

Figure 5. SEM microstructures of (a) 5 wt % CNFs/VM1 and (b) 5 wt % CNFs/VM2; (c) and (d) are the enlarged area images of (a) and (b), respectively.

of magnitude. With the increase of the CNF loading, the interfacial area between conductive CNFs and nonconductive VM matrix is significantly enhanced, where the charge carriers accumulate and thus lead to a significant increase of the permittivity. In addition, higher CNF loading also provides more chances for the CNFs to contact each other or narrows the distance among the CNFs, which facilitates the electron transportation within the composites and decreases the resistivity.

3.3. Stretching Resistivity. The piezoresistive response of the CNTs[13,43,44] and their PNCs, like epoxy/CNTs PNCs[45,46] as well as CNFs-based PNCs like polypropylene (PP),[21] has opened a variety of sensing applications. Figure 6 shows the resistivity change in the PNCs during the cyclic stretching deformation with continuous cyclic loading. It is observed from the graph that the instantaneous response of the resistivity change closely follows the change of the strains, which indicates that the resistivity of the specimen changes with the applied strains. This piezoresistive behavior is due to the nanoscale structural change in the percolation and corresponds to a stochastic separation of the conducting pathways owing to the increased matrix strain.

It is well established that the fibers are oriented orthogonal to the direction of the applied load during the tensile deformation.[47] The crack propagates in the polymer matrix either among the nanofibers or the interfaces between the nanofiber and matrix, as evidenced by the SEM images in Figure 7a,b. Once the crack initiates in the composites, the stress will redistribute along the nanofibers and the cracks continue to develop with the increase of the applied load. A 120% strain is applied for the first cycle, and it is observed that the specimens are not able to recover to the original length. In other words, a permanent change of about 40% strain in deformation is remained and the corresponding resistivity is increased by around 2 orders of magnitude

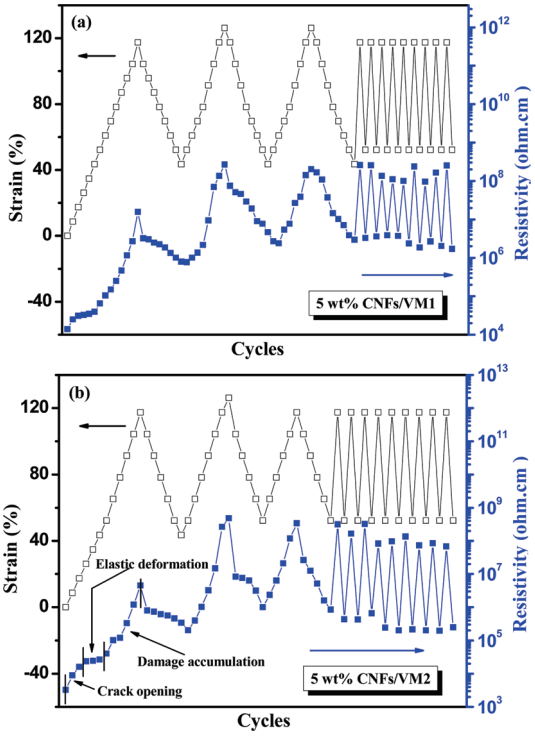

Figure 6. Cyclic strain applied to specimen and the instantaneous response of resistivity with strain of (a) 5 wt % CNFs/VM1 and (b) 5 wt % CNFs/VM2 PNCs.

(10^4–10^6 ohm·cm for CNFs/VM1 and 10^3–10^5 ohm·cm for CNFs/VM2). This large difference in the deformation

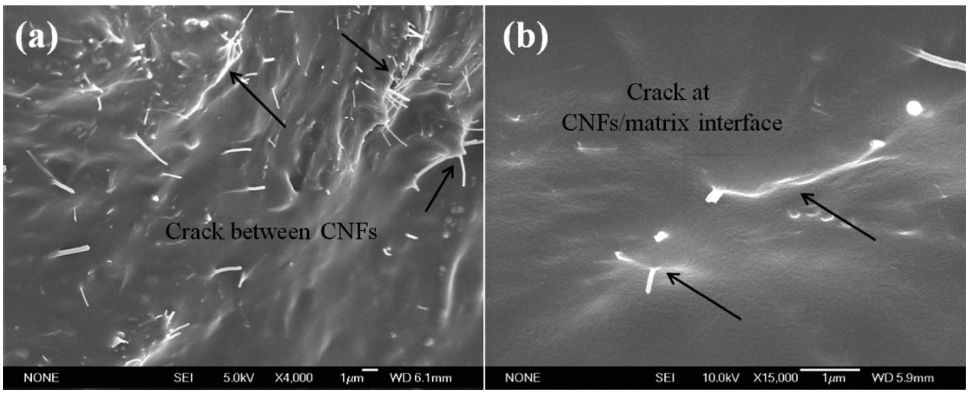

Figure 7. SEM of the crack propagation between (a) CNFs and (b) CNFs/matrix interface.

represents a combined process of the polymer chain stretching relaxation and the accumulation of the structural damages within the composites, which also reveal the mechanism of the resistivity change. Note also that this 120% reversible strain is much larger than the reported maximum achievable strain at break of the multiwalled CNT (MWCNT)/elastomeric polyurethane (PU) composites with a 5 wt % tube loading, which show only a 25% strain.[48] Meanwhile, the observed strain-induced resistance sensitivity (R/R_0, R is the resistivity at specific strain and R_0 is the resistivity without strain) of about 100 is much larger than the reported 1.5 at 100% strain in the CNT forest/PU composites.[22] During the first two cycles, the response of resistivity did not follow a linear mode after a linear strain was applied. The resistivity curve on the first-cycle strain can be divided into three stages: crack opening, elastic deformation, and damage accumulation (Figure 6b). The experimental results are quite similar to the observations in the CNTs/epoxy PNCs.[45] The resistivity of the second cycle is relatively higher than that of the first cycle, which means that some conducting pathways are irreversibly damaged. After the second cycle, the resistivity of 5 wt % CNF/VM1 PNCs is almost stabilized even though slight deviation is still observed. However, the resistivity is getting lower with increasing cycle number for the 5 wt % CNF/VM2 PNCs, indicating some conduction pathways are re-formed during the cyclic loading.

3.4. Thermal Gravimetric Analysis. As nanofillers, CNTs,[49] CNFs,[50] carbon,[51] iron nanoparticles,[52] and quantum dots[53] are generally reported to induce an improved thermal stability in their corresponding PNCs relative to their pure polymers. Especially, the decomposition temperature, T_d, and the temperature of the maximum weight loss rate, T_{peak}, are higher in the PNCs. Thermogravimetric analysis (TGA) of the CNFs/VM PNCs was carried out in air and the thermograms are shown in Figure 8. Two degradation stages are observed for both VM1 and VM2 (Figure 8). The first stage within 250−350 °C corresponds to the degradation of polypropylene[54] and the second stage within 350−550 °C indicates the degradation of polyethylene (PE).[55] The different fraction of ethylene leads to the thermal property difference between pure VM1 and pure VM2. The higher fraction of ethylene reduces the thermal stability of propylene portion in the elastomers. Therefore, a lower degradation temperature is observed in VM1 and a higher degradation temperature is observed in VM2. The addition of the CNFs did not influence the initial decomposition temperature of VM1 and VM2. However, the residue fraction of the degradation of VM increased after the incorporation of

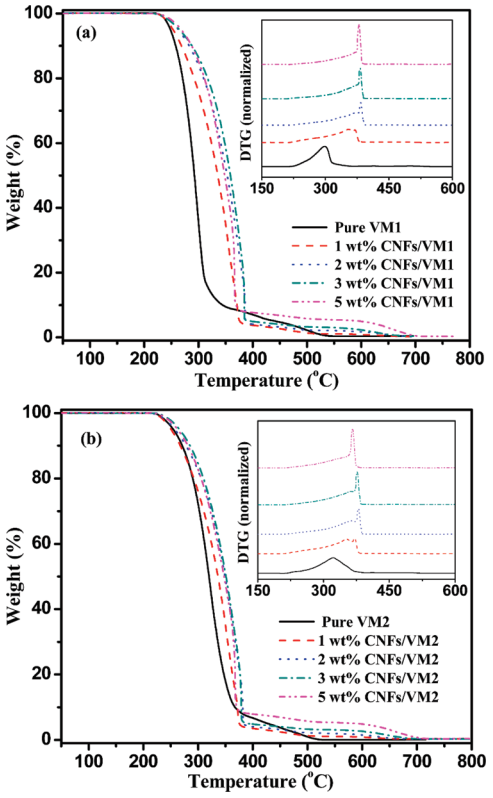

Figure 8. TGA curves of (a) CNFs/VM1 and (b) CNFs/VM2 PNCs.

CNFs. This implies that the CNFs induce a stabilization of VM during the final stages of the degradation process. The 20 wt % weight loss temperature $T_{20\%}$ and T_{peak} are summarized in Table 1. The highest $T_{20\%}$ and T_{peak} are observed at the weight ratio of 3 and 2 wt % in CNFs/VM1 and CNFs/VM2 PNCs, respectively. As the CNF loading further increases to 5 wt %, the thermal stability degrades due to the damage to the continuity of the polymer phase. The 3 wt % CNFs/VM1 PNCs show a 45.9 °C shift in $T_{20\%}$ as compared to that of the pure VM1, and a much higher T_{peak} shift of 86 °C is observed in the composites with a CNF loading of 2 wt %. The enhancement of $T_{20\%}$ and T_{peak} in the CNFs/VM2 PNCs is much lower with the same CNF loadings, which exhibits a value of 19.6 and 56.7 °C, respectively. Dispersed CNFs restrict the segmental motion of the polymer

Table 1. Thermal Properties of Pure VM and Its CNFs/VM Nanocomposites

compositions	$T_{20\%}$	T_{peak}	T_g (°C)	T_m (°C)	ΔH_m (J/g)
pure VM1	270.9	298.0	47.5	111.1	4.58
1 wt % CNFs/VM1	291.9	354.4	45.4	110.9	4.88
2 wt % CNFs/VM1	309.6	384.0	45.1	109.6	4.62
3 wt % CNFs/VM1	316.8	382.2	44.7	109.0	4.32
5 wt % CNFs/VM1	310.8	379.6	46.2	108.9	4.21
pure VM2	290.2	323.3	45.5	108.5	4.49
1 wt % CNFs/VM2	292.1	352.9	46.4	110.4	5.02
2 wt % CNFs/VM2	305.6	380.0	46.5	111.1	5.17
3 wt % CNFs/VM2	309.8	376.6	46.2	110.2	5.01
5 wt % CNFs/VM2	305.6	366.4	49.1	110.8	4.50

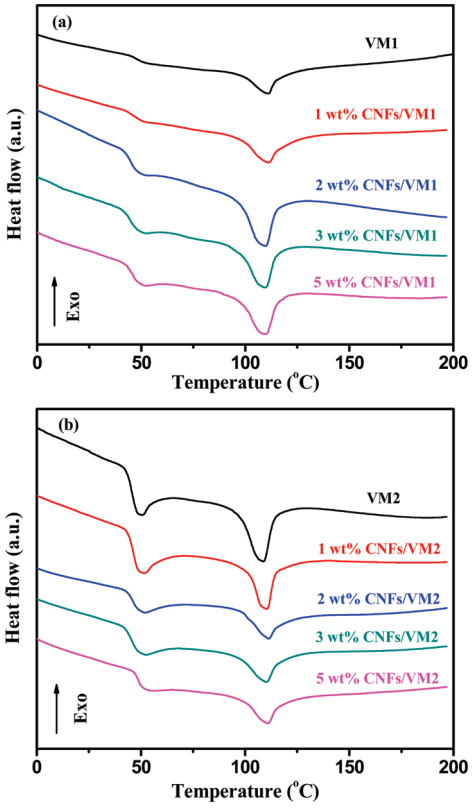

Figure 9. DSC curves of (a) CNFs/VM1 and (b) CNFs/VM2 PNCs.

chains and thereby delay the decomposition of the PNCs. Polymers near the CNFs degrade more slowly, which would shift the T_{peak} to a higher temperature.[39] Excluding the difference of the two polymers, the enhancement of thermal stability ($T_{20\%}$ and T_{peak}) induced by CNFs are nearly identical in both composite systems.

3.5. Differential Scanning Calorimetry. The DSC spectra from the first heating process for the pure VM and the nanocomposites with different CNFs contents are presented in Figure 9. The first cooling and second heating processes are conducted to investigate the crystalline behavior and thermal history effect on the composite performance. The results show that no specific peaks are observed in the cooling process and only one broad melting peak appears on the second heating process (not plotted in the figure). The glass transition temperatures (T_g) for all specimens are determined from the midpoints of the corresponding glass transition regions. The measured T_g, melting temperature (T_m) and melting enthalpy (ΔH_m) values are listed in Table 1. The increasing CNF content results in a shift of T_g (T_m) to lower temperatures for the CNFs/VM1 PNCs, while a shift to higher temperatures is observed for the CNFs/VM2 PNCs. The increased T_g (T_m) in the PNCs derives from the restriction effect of the CNFs on the segmental mobility of VM2. This effect is relatively weak since the polymer chain of VM1 is tougher than that of VM2, as stated by the higher T_g and T_m in Table 1.

From DSC analysis, an increased crystallinity is deduced in the VM1 PNCs (1 and 2 wt % fiber loading) and VM2 PNCs (1−5 wt % fiber loading) than that of pure VM (Table 1), which is determined from the increased melting enthalpy (ΔH_m) of the PNCs and is consistent with the recently reported increased crystallinity in the CNFs/PP nanocomposites.[56] However, to an elastomer, the contribution of each specific propylene and ethylene component to the increased crystallinity is very difficult to identify since both are crystalline. The fusion enthalpy for a theoretically 100% crystalline PP is 209 J/g[57] and 288.9 J/g for a 100% crystalline PE,[58] which explains well the slightly higher melting enthalpy (ΔH_m, 4.58 J/g) of VM1 than that of VM2 (4.49 J/g) owing to the larger fraction of ethylene part in VM1. At the same fiber loading, though, a large enthalpy discrepancy is observed in these two elastomeric composite systems than that in the two pure elastomers. To be more specific, VM2 composites exhibit larger ΔH_m (more crystalline fraction) than that of VM1 composites. This indicates that CNFs play a more important role in the VM2 crystallization than that in VM1 composites.

4. CONCLUSIONS

This work presents an electrically conductive polymer nanocomposite that can be utilized as strain sensors with large mechanical deformation. The resistivity is reversibly changed by 10^2-10^3 times upon stretching to 120% strain and recovery to 40% strain. The sensitivity (resistivity change upon strain) of the CNFs/VM2 PNCs is better than that of the CNFs/VM1 PNCs where the resistivity changes more significantly upon applying the same strain. Lower percolation threshold (1 wt %) is observed in the CNFs/VM2 PNCs than that (3 wt %) in the CNFs/VM1 PNCs, which is attributed to the better CNF dispersion quality in VM2 as evidenced by the SEM observations. Negative permittivity and dielectric loss (tan δ) peak are observed in both CNFs/VM1 and CNFs/VM2 composite systems at above each percolation threshold, indicating that the internal electron conduction pathways have been constructed and thus lead to a significant reduction in the resistivity. TGA results reveal an improved thermal stability in the PNCs relative to that of pure polymers. The glass transition behavior differs in the opposite way in the two composites systems. To be specific, the glass transition and melting temperatures are lower in the CNFs/VM1 PNCs than that of pure VM1, while in CNFs/VM2, these two characteristic temperatures are higher than those of pure VM2.

AUTHOR INFORMATION

Corresponding Author

*E-mail: zhanhu.guo@lamar.edu. Phone: (409) 880-7654.

■ ACKNOWLEDGMENT

This project is supported by the National Science Foundation-Nanoscale Interdisciplinary Research Team and Materials Processing and Manufacturing (CMMI-1030755). The elastomers supplied from ExxonMobil Chemical Co. are greatly appreciated.

■ REFERENCES

(1) Pelrine, R.; Kornbluh, R.; Pei, Q.; Joseph, J. *Science* **2000**, *287*, 836–839.
(2) Pradhan, B.; Setyowati, K.; Liu, H.; Waldeck, D. H.; Chen, J. *Nano Lett.* **2008**, *8*, 1142–1146.
(3) An, K. H.; Jeong, S. Y.; Hwang, H. R.; Lee, Y. H. *Adv. Mater.* **2004**, *16*, 1005–1009.
(4) Zhu, J.; Wei, S.; Ryu, J.; Sun, L.; Luo, Z.; Guo, Z. *ACS Appl. Mater. Interfaces* **2010**, *2*, 2100–2107.
(5) Zhu, J.; Wei, S.; Alexander, M., Jr.; Dang, T. D.; Ho, T. C.; Guo, Z. *Adv. Func. Mater.* **2010**, *20*, 3076–3084.
(6) Zhu, J.; Wei, S.; Alexander, M., Jr; Cocke, D.; Ho, T. C.; Guo, Z. *J. Mater. Chem.* **2010**, *20*, 568–574.
(7) Lendlein, A.; Jiang, H.; Junger, O.; Langer, R. *Nature* **2005**, *434*, 879–882.
(8) Cho, J. W.; Kim, J. W.; Jung, Y. C.; Goo, N. S. *Macromol. Rapid Commun.* **2005**, *26*, 412–416.
(9) Neoh, K. G.; Tan, K. K.; Goh, P. L.; Huang, S. W.; Kang, E. T.; Tan, K. L. *Polymer* **1999**, *40*, 887–893.
(10) Hilczer, B.; Kulek, J.; Markiewicz, E.; Kosec, M.; Malic, B. *J. Non-Cryst. Solids* **2002**, *305*, 167–173.
(11) Vinogradov, A.; Su, J.; Jenkins, C.; Bar-Cohen, Y. *Mater. Res. Soc. Symp. Proc.* **2006**, *889*, 51–56.
(12) Baughman, R. H.; Zakhidov, A. A.; de Heer, W. A. *Science* **2002**, *297*, 787–792.
(13) Tombler, T. W.; Zhou, C.; Alexseyev, L.; Kong, J.; Dai, H.; Liu, L.; Jayanthi, C. S.; Tang, M.; Wu, S.-Y. *Nature* **2000**, *405*, 769–772.
(14) Li, Z.; Dharap, P.; Nagarajaiah, S.; Barrera, E. V.; Kim, J. D. *Adv. Mater.* **2004**, *16*, 640–643.
(15) Stampfer, C.; Helbling, T.; Obergfell, D.; Schöberle, B.; Tripp, M. K.; Jungen, A.; Roth, S.; Bright, V. M.; Hierold, C. *Nano Lett.* **2006**, *6*, 233–237.
(16) Thostenson, E. T.; Chou, T. W. *Adv. Mater.* **2006**, *18*, 2837–2841.
(17) Gao, L.; Thostenson, E. T.; Zhang, Z.; Chou, T.-W. *Carbon* **2009**, *47*, 1381–1388.
(18) Tibbetts, G. G.; Lake, M. L.; Strong, K. L.; Rice, B. P. *Compos. Sci. Technol.* **2007**, *67*, 1709–1718.
(19) Zhu, J.; Wei, S.; Ryu, J.; Budhathoki, M.; Liang, G.; Guo, Z. *J. Mater. Chem.* **2010**, *20*, 4937–4948.
(20) Zhu, J.; Wei, S.; Yadav, A.; Guo, Z. *Polymer* **2010**, *51*, 2643–2651.
(21) Paleo, A. J.; Van Hattum, F. W. J.; Pereira, J.; Rocha, J. G.; Silva, J.; Sencadas, V.; Lanceros-Méndez, S. *Smart Mater. Struct.* **2010**, *19*, 065013.
(22) Shin, M. K.; Oh, J.; Lima, M.; Kozlov, M. E.; Kim, S. J.; Baughman, R. H. *Adv. Mater.* **2010**, *22*, 2663–2667.
(23) Laraba-Abbes, F.; Ienny, P.; Piques, R. *Polymer* **2003**, *44*, 821–840.
(24) Lee, K.; Lee, B.; Kim, C.; Kim, H.; Kim, K.; Nah, C. *Macromol. Res.* **2005**, *13*, 441–445.
(25) Knite, M.; Teteris, V.; Kiploka, A.; Kaupuzs, J. *Sens. Actuators, A* **2004**, *110*, 142–149.
(26) Hoffman, A. J.; Alekseyev, L.; Howard, S. S.; Franz, K. J.; Wasserman, D.; Podolskiy, V. A.; Narimanov, E. E.; Sivco, D. L.; Gmachl, C. *Nat. Mater.* **2007**, *6*, 946–950.
(27) Pendry, J. B.; Holden, A. J.; Stewart, W. J.; Youngs, I. *Phys. Rev. Lett.* **1996**, *76*, 4773.
(28) Dolgov, O. V.; Kirzhnits, D. A.; Maksimov, E. G. *Rev. Mod. Phys.* **1981**, *53*, 81.
(29) Chui, S. T.; Hu, L. *Phys. Rev. B* **2002**, *65*, 144407.
(30) Zhu, J.; Wei, S.; Zhang, L.; Mao, Y.; Ryu, J.; Karki, A. B.; Young, D. P.; Guo, Z. *J. Mater. Chem.* **2011**, *21*, 342–348.
(31) Zhu, J.; Wei, S.; Zhang, L.; Mao, Y.; Ryu, J.; Mavinakuli, P.; Karki, A. B.; Young, D. P.; Guo, Z. *J. Phys. Chem. C* **2010**, *114*, 16335–16342.
(32) Li, B.; Sui, G.; Zhong, W.-H. *Adv. Mater.* **2009**, *21*, 4176–4180.
(33) Xing, H.; Sun, L.; Song, G.; Gou, J.; Hao, Y. W. *Nanotechnology* **2008**, *19*, 025704.
(34) Legros, F.; Fourrier-Lamer, A. *Mater. Res. Bull.* **1984**, *19*, 1109–1117.
(35) Liu, C.-D.; Lee, S.-N.; Ho, C.-H.; Han, J.-L.; Hsieh, K.-H. *J. Phys. Chem. C* **2008**, *112*, 15956–15960.
(36) Tamura, R.; Lim, E.; Manaka, T.; Iwamoto, M. *J. Appl. Phys.* **2006**, *100*, 114515.
(37) Dang, Z. M.; Wang, L.; Yin, Y.; Zhang, Q.; Lei, Q. Q. *Adv. Mater.* **2007**, *19*, 852–857.
(38) Du, F.; Scogna, R. C.; Zhou, W.; Brand, S.; Fischer, J. E.; Winey, K. I. *Macromolecules* **2004**, *37*, 9048–9055.
(39) Moniruzzaman, M.; Winey, K. I. *Macromolecules* **2006**, *39*, 5194–5205.
(40) Balberg, I.; Anderson, C. H.; Alexander, S.; Wagner, N. *Phys. Rev. B* **1984**, *30*, 3933.
(41) Barrau, S.; Demont, P.; Perez, E.; Peigney, A.; Laurent, C.; Lacabanne, C. *Macromolecules* **2003**, *36*, 9678–9680.
(42) Sandler, J. K. W.; Kirk, J. E.; Kinloch, I. A.; Shaffer, M. S. P.; Windle, A. H. *Polymer* **2003**, *44*, 5893–5899.
(43) Cao, J.; Wang, Q.; Dai, H. *Phys. Rev. Lett.* **2003**, *90*, 157601.
(44) Minot, E. D.; Yaish, Y.; Sazonova, V.; Park, J.-Y.; Brink, M.; McEuen, P. L. *Phys. Rev. Lett.* **2003**, *90*, 156401.
(45) Thostenson, E. T.; Chou, T. W. *Nanotechnology* **2008**, *19*, 215713.
(46) Hu, N.; Karube, Y.; Yan, C.; Masuda, Z.; Fukunaga, H. *Acta Mater.* **2008**, *56*, 2929–2936.
(47) Chou, T.-W. *Microstructural Design of Fiber Composites*; Cambridge University Press: Cambridge, UK, 1992.
(48) Sahoo, N. G.; Jung, Y. C.; Yoo, H. J.; Cho, J. W. *Compos. Sci. Technol.* **2007**, *67*, 1920–1929.
(49) Ge, J. J.; Hou, H.; Li, Q.; Graham, M. J.; Greiner, A.; Reneker, D. H.; Harris, F. W.; Cheng, S. Z. D. *J. Am. Chem. Soc.* **2004**, *126*, 15754–15761.
(50) Zhu, J.; Wei, S.; Ryu, J.; Budhathoki, M.; Liang, G.; Guo, Z. *J. Mater. Chem.* **2010**, *20*, 4937–4948.
(51) Vassiliou, A.; Bikiaris, D.; Chrissafis, K.; Paraskevopoulos, K. M.; Stavrev, S. Y.; Docoslis, A. *Compos. Sci. Technol.* **2008**, *68*, 933–943.
(52) Zhu, J.; Wei, S.; Rutman, D.; Haldolaarachchige, N.; Young, D. P.; Guo, Z. *Polymer* **2011**, *52*, 2947–2955.
(53) Zhu, J.; Wei, S.; Patil, R.; Rutman, D.; Kucknoor, A. S.; Wang, A.; Guo, Z. *Polymer* **2011**, *52*, 1954–1962.
(54) Qin, H.; Zhang, S.; Zhao, C.; Hu, G.; Yang, M. *Polymer* **2005**, *46*, 8386–8395.
(55) Gorrasi, G.; Di Lieto, R.; Patimo, G.; De Pasquale, S.; Sorrentino, A. *Polymer* **2011**, *52*, 1124–1132.
(56) Chen, X.; Wei, S.; Yadav, A.; Patil, R.; Zhu, J.; Ximenes, R.; Sun, L.; Guo, Z. *Macromol. Mater. Eng.* **2011**, *296*, 434–443.
(57) Yuan, Q.; Misra, R. D. K. *Polymer* **2006**, *47*, 4421–4433.
(58) Failla, M. D.; Vallés, E. M.; Lyons, B. J. *J. Appl. Polym. Sci.* **1999**, *71*, 1375–1384.